Thermal Isostasy: Using Remote Geophysical Data to Model Antarctic Surface Heat Flow

Thesis submitted in accordance with the requirements of the University of Adelaide for an Honours Degree Geophysics

Matthew Lawrence Linke

April 2020

THE UNIVERSITY of ADELAIDE

Thermal 'Ice'-ostasy: Using Remote Geophysical Data to Model Antarctic Surface Heat Flow

Thermal Isostasy and Antarctic Heat Flow

ABSTRACT

Antarctica is host to the world's largest terrestrial ice sheets. Due to concerns about changing global climate and resultant sea level change, the thermal stability of the ice sheets is important, yet poorly understood. Geothermal heat flow in Antarctica is a vital geophysical parameter in understanding the stability and movement of the overlying ice sheets. Conventional heat flow methods have not been reliable as the ice sheets have hindered the accessibility of surface rocks. This, coupled with the cost associated with the remoteness and hostility of the environment, means little data has been collected. Thus, geothermal heat flow is estimated with geophysical proxies. In this study, the principles of compositional and thermal isostasy are utilised to estimate the geothermal heat flow of Antarctica. Elevation, seismic velocity and geochemical data have been used to construct isostatic models of the Antarctic ice sheets and crust; this allows for isolation of the thermal component of isostatic elevation. Modelled geothermal gradients, incorporating geochemical, magnetic and seismic data, are then used to calculate a modelled thermal elevation. The two thermal elevations are then compared and the heat flow from the thermal model is taken as the geothermal heat flow. The first pass of this model computes moderate discrepancies between modelled thermal elevations and calculates very high geothermal heat flow, with a continental average of 92 mW/m^2. Despite this, broad geological trends are observed in this model agree with existing geological and tectonic knowledge. The errors present are likely due to issues in the modelling of geothermal proxies and isostatic assumptions. Though these results are not ideal, this model was successful in execution and serves as a proof of concept for further thermal isostatic modelling. With further refinement of the geophysical proxies and integration of more data types, this model may serve as a starting point for more integrated remote geophysical modelling of the thermal properties of the Antarctic lithosphere.

KEYWORDS

Thermal isostasy, heat flow, Antarctica, isostasy, geophysics, geothermal

Table of Contents

List of Figures

List of Tables

INTRODUCTION

Antarctica is host to the world's largest ice sheets. In Antarctica, surface heat flow is an important geophysical parameter due to its impact on the stability and movement of the overlying ice sheets (Shapiro & Ritzwoller 2004). With concerns about changing global climate and how warming may impact sea levels, an understanding of the thermal stability of global ice sheets is becoming increasingly pertinent (Shepherd et al., 2012). Despite its importance in glacial modelling, it remains poorly constrained due to the hostility and remoteness of the continent. Existing measurements around the Antarctic coast give insight into the heat flux, but observations are sparse and yield unreliable estimates of conductive heat flux due to ice dynamics (Blackman et al., 1987; Bücker et al., 2000; Bücker et al., 2001; Dziadek et al., 2019).

Due to the logistical challenges associated with Antarctic research, it is necessary to resort to modelling geothermal heat flow using remote geophysical data. Existing work to estimate geothermal heat flux based on magnetic surveys (Martos et al., 2017; Maule et al., 2005), seismic data (O'Donnell et al., 2019; Shapiro & Ritzwoller 2004) and gravity surveys (Block et al., 2009) produces reasonable results, with some studies considering multiple parameters in their models (Haeger et al., 2019; Pappa et al., 2019).

Isostasy is a geological phenomenon that occurs due to hydrostatic equilibrium between lateral differing densities of crustal material floating on a plastically deforming mantle (Watts 2011). Much of Antarctica's bedrock is below sea level due to isostatic compensation from ice loading (Figure 1; Fretwell et al., 2013). Differing densities arise from variations in compositional and thermal properties, giving rise to elevation changes (Chapman & Hasterok 2011). Thermal isostasy has also been successfully applied to continental settings and shown to account for significant el-

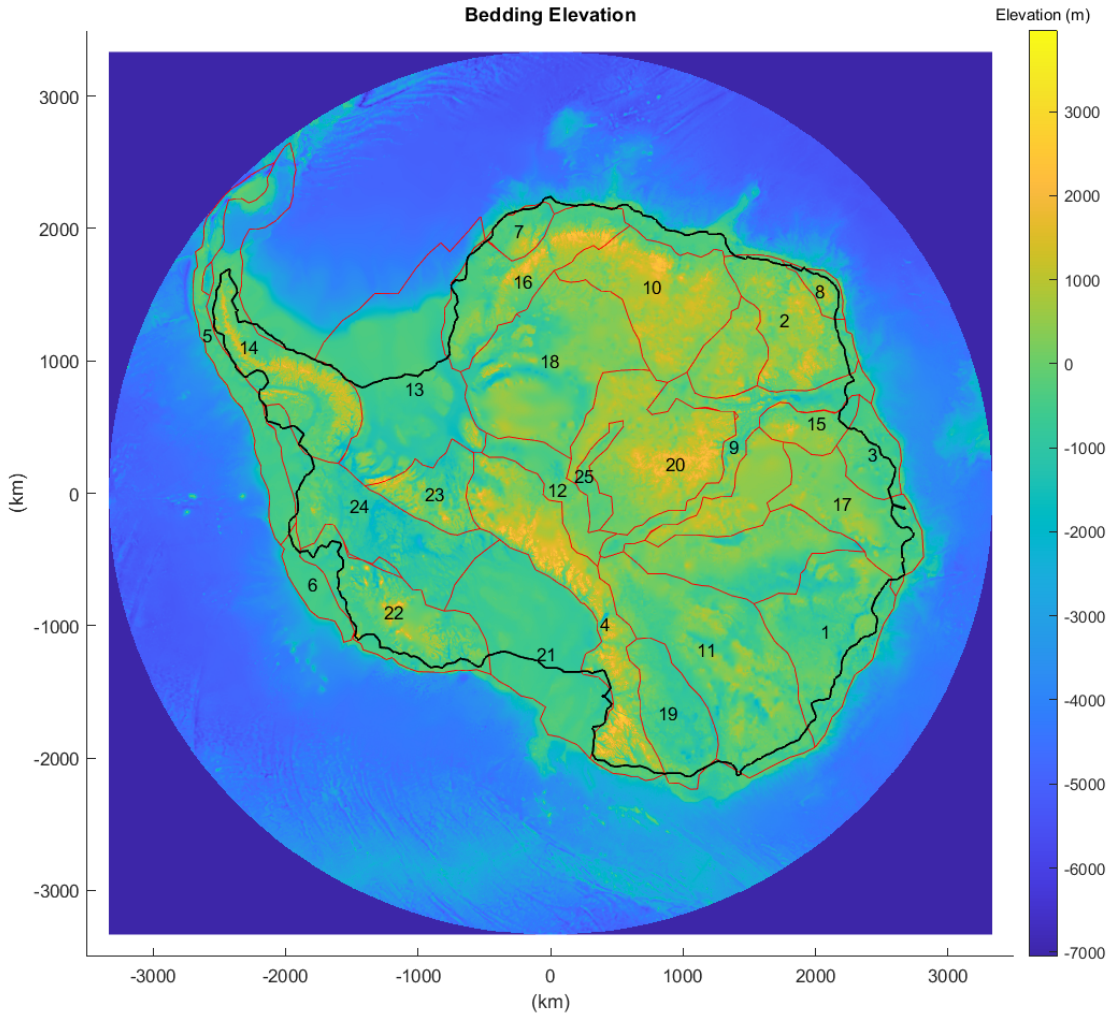

Figure 1: Bedmap2 (Fretwell et al., 2013) dataset for bedrock elevation. Coastline is shown in bold black, while identified geological provinces are outlined in red. These are listed in accordance with Table 1.

evation changes once correcting for compositional density variation (Hasterok & Chapman 2007a; Hasterok & Chapman 2007b; Chapman & Hasterok 2011).

Based on the existing work on heat flow modelling and thermal isostasy (An et al., 2015; Hasterok & Chapman 2007a; Hasterok & Chapman 2007b; Hasterok & Chapman 2011; Martos et al., 2017), two hypotheses are drawn. Firstly, the thermal state of the lithosphere is the main control on elevation on a continental scale resolution after compositional density corrections. Secondly, Curie depth estimates from magnetic studies provide an accurate constraint on internal crustal temperatures.

Furthermore, testing of these hypotheses will show that geothermal heat flow can be modelled using compositionally corrected elevation and Curie depth estimates.

This study aims to constrain geothermal gradients using existing magnetic and shear velocity models in order to construct thermal isostatic models that match observed elevations. Corrections are made for mass loading by ice sheets and lithospheric composition using seismic velocity models as a proxy for density. This shear velocity model is also used to estimate thermal conductivity and heat production. Broad scale geographic variations in thermal properties are identified throughout the Antarctic crust.

BACKGROUND

Heat Flow

Geothermal heat flow in the Antarctic context is poorly constrained by physical measurements. Work exists utilising seismic and magnetic data as proxies to further constrain geothermal heat flow, but results disagree. Furthermore, tectonic reconstructions may yield reasonable estimates of geothermal heat flow around the periphery from observations on conjugate margins.

HEAT FLOW OBSERVATIONS

Much work exists on geothermal heat flow of Antarctica, but is often constrained to the coastline or the Trans Antarctic Mountains. Additionally, the data is often unreliable due to the logistical hurdles associated with hostile conditions. An early project undertaken in the Ross Sea indicated heat flow of between 66 to 73 mW/m^2 which was associated with an extensional regime in the area (Blackman et al., 1987). Further offshore drilling on ice sheets in the Ross Sea has yielded average estimates of 60 mW/m^2 (Bücker et al., 2001) as well as constructing local geotherms (Bücker et al., 2000), again agreeing with high heat flow in the area. Sediment probes deployed

on the continental shelf in the Amundsen Sea Embayment found elevated heat flux of between 65 to 95 mW/m^2 (Dziadek et al., 2019). Ice penetrating radar studies of subglacial lakes, utilised in tandem with knowledge of ice sheet velocities, have been used near the South Pole to estimate anomalously large geothermal heat flows of up to 120 mW/m^2 (Jordan et al., 2018). However, much of this data is riddled with various experimental issues (Blackman et al., 1987, Bücker et al., 2000, Bücker et al., 2001) as well as being limited to predominantly offshore locales.

HEAT FLOW PROXIES

Poor comparisons between proxies such as magnetic and seismic datasets and conjugate data points suggests these methods suffer from various experimental issues (Figure 2), increasing the need for better heat production and heat flow models.

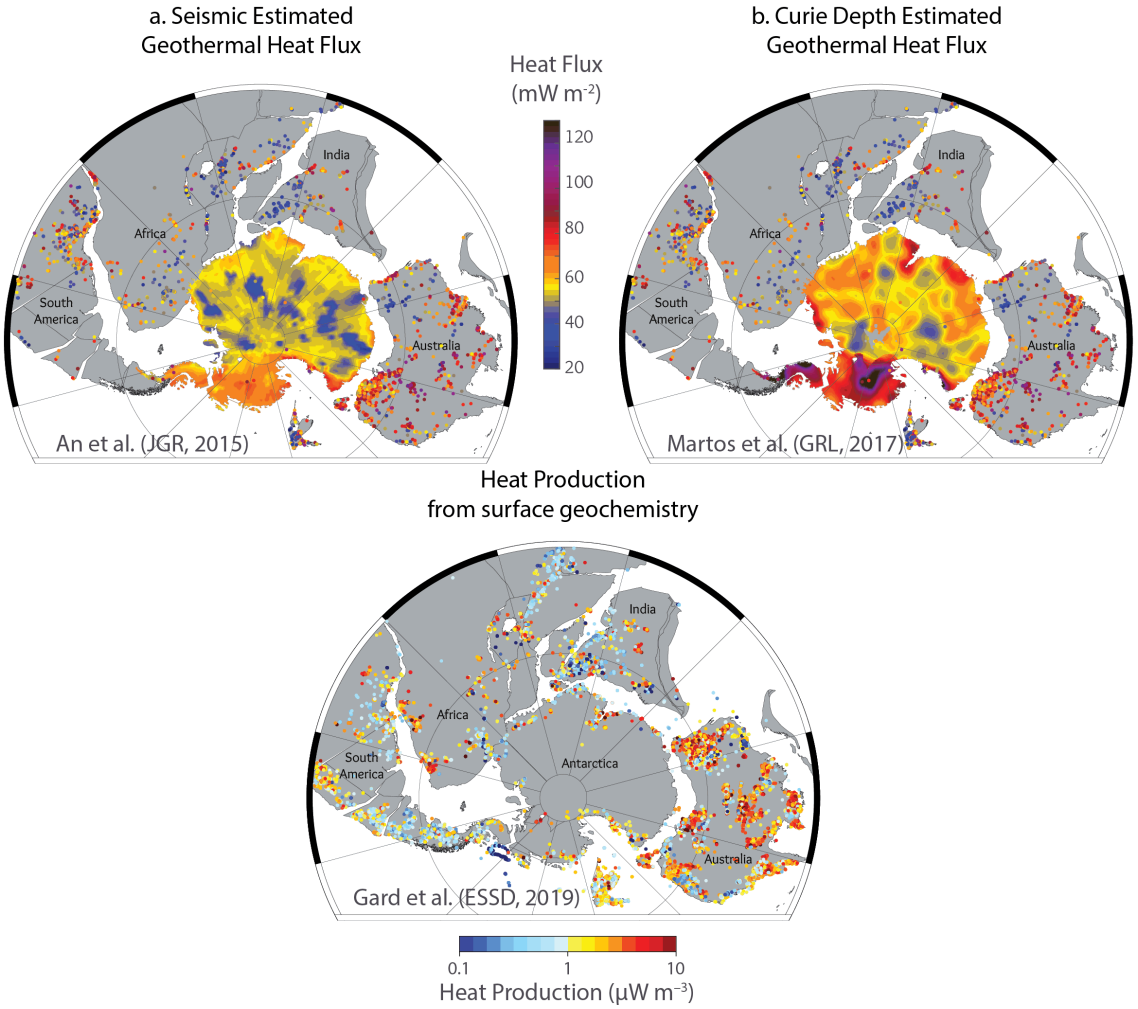

Figure 2: Plate reconstructions at 200 Ma with present day geothermal heat flow (a, b) and heat production (c) superimposed. Note the difference between modelled heat flow estimates from seismic (a) and magnetic (b) methods and heat flow on conjugate margins. Correlation along continental margins is not observed with either model. However, heat production from Gard et al., (2019) does seem to generally match along the margins (c). Modified from Hasterok et al., (2019).

SEISMIC

Seismic velocities are dependent on temperature, pressure and composition. Pressure and shear waves are sensitive to these parameters differently, with shear waves being the most susceptible to temperature. Within the mantle, compositional variations are relatively small, and therefore temperature is the largest contributor to lateral variations in shear velocity (Hansen et al., 2014, An et al., 2015). This temperature dependence permits the use of seismic data to infer the thermal state of the lithosphere. An et al., (2015) applied this method to compute temperature in the upper mantle within Antarctica and calculate a 1-D steady-state heat conduction model. The equation defining steady-state thermal conduction is:

$$\nabla . k \nabla T = -A \tag{1}$$

where A and k are heat production ($\mu \mathrm{Wm}^{-3}$) and thermal conductivity ($\mathrm{Wm}^{-1}\mathrm{K}^{-1}$) respectively. While Equation 1 is the governing differential equation, it is usually applied to a layered model defined by:

$$T_i = T_{i-1} + \frac{q_{i-1}}{k_i}(z_i - z_{i-1}) - \frac{A_i}{2k_i}(z_i - z_{i-1})^2 \tag{2}$$

$$q_i = q_{i-1} - A_i(z_i - z_{i-1}) \tag{3}$$

where i is the ith layer, T is temperature (°C), q is heat flow ($\mathrm{mW/m}^2$), k is thermal conductivity ($\mathrm{Wm}^{-1}\mathrm{K}^{-1}$), z is the depth to the base of the layer (m) and A is heat production ($\mu \mathrm{Wm}^{-3}$). It is important to note that T and q are calculated at the interface between layers at z, while k and A are properties of the whole layer. In this model, boundary conditions for this steady state are the mantle temperatures computed with seismic velocities and a surface temperature (T_0) of

0°C. Applying these conditions allows for the construction of thermal models. These thermal models identify heat flow estimates above the global continental average of 65 mW/m^2 (Figure 2) in Western Antarctica yet below the average in Eastern Antarctica. The discrete velocity change at the Mohorovičić discontinuity (Moho) is also easily detectable, making seismic data useful for mapping the Moho depth (Baranov & Morelli 2013; Haeger et al., 2019).

MAGNETICS

The maximum depth of magnetisation of Earth materials provides a temperature constraint in the lithosphere (Martos et al., 2017). Assuming the main source of magnetism in the crust is magnetite, which has a Curie temperature of 580°C, a steady state geothermal model can be constructed and heat flow through the area can be determined. This method is often utilised for geothermal energy (Elbarbary et al., 2018; Quintero et al., 2019). 1-D steady-state conductive heat flow models (mathematically similar to Equations (1), (2) and (3)) utilising Curie depth models from airborne magnetic data have produced heat flow estimates agreeing with known regional geology (Martos et al., 2017). These models found a regional average of 68 mW/m^2 with values ranging from 42 to 180 mW/m^2. While regional trends seem consistent with known geological features, areas of anomalously high heat flow exist.

CONSTRAINTS FROM RECONSTRUCTIONS

It may be feasible to estimate geothermal heat flow along some coastal provinces by analysing conjugate margins. By measuring geothermal heat flow in accessible areas that were once spatially adjacent to Antarctica as well as utilising current tectonic reconstructions of Gondwana, reasonable estimates of geothermal heat flow (50 to 75 mW/m^2) in Antarctica can be attained (Pollett et al., 2019). However, such methods are useful for the edges of the continent but are currently limited throughout Antarctica due to the relative lack of knowledge of regional geology (Pollett et al., 2019). These methods also require that neither side of the conjugate

margin involved in the comparison has been affected by thermal disturbances during or post separation.

Contributions to Elevation

Observed elevation is a combination of buoyancy, strength and dynamic forces that act on the lithosphere. Hasterok and Chapman (2007a) suggest observed elevation can be separated into individual components as:

$$\varepsilon_{observed} = \Delta\varepsilon_{compositional} + \Delta\varepsilon_{thermal} + \Delta\varepsilon_{H_2O} + \Delta\varepsilon_{geodynamic} + \Delta\varepsilon_{flexural} \qquad (4)$$

where ε denotes elevation and the terms on the right hand side are each of its appropriate components. Equation (4) suggests the thermal component of elevation can be isolated. For the scope of this study, flexural and geodynamic elevations are assumed to be negligible; however, these assumptions may lead to errors. Gvirtzman et al., (2016) investigated mid-ocean ridges and hotspots in order to constrain a maximal sub-lithospheric geodynamic elevation of approximately 1 km.

COMPOSITION

Compositional buoyancy accounts for approximately 3 km of elevation variations in the continental crust (Hasterok & Chapman, 2007b) and arises from a large variety of minerals present. Thus, the isostatic effect of elevation in continental settings tends to be dominated by compositional variations in density (Hasterok & Chapman 2007a). Hasterok & Chapman (2007b) utilise a correction for compositional effects on elevation using V_p models and an empirical velocity to density conversion.

Compositional variations within the mantle are far less extreme than in the crust and have not been considered in the present study. However, compositional variations may still occur and could lead to noticeable errors. Goes (2002) found a 1% decrease

in iron content (Mg number 89 to 90 where Mg number is defined by $\frac{Mg+Fe}{Mg}$) from the Moho to 250 km depth beneath the Canadian Shield could contribute to 1 km of elevation, indicating significant mantle variations beneath Antarctica could cause considerable changes in elevation.

THERMAL

Most of the Earth's materials expand when heated, reducing density and increasing buoyancy. This resultant density change can be significant enough to account for up to 3 kilometres of elevation, most notably observed in ocean bathymetry (Chapman & Hasterok 2011). A similar magnitude of elevation change, due to variations in the lithospheric thermal state, can also be seen in continental crust once adjustments for compositional density variations are applied. In North America, compositionally adjusted elevations reveal a clear trend of up to 3 km difference between cold and hot regions (Hasterok & Chapman 2007b). However, a different application of the same technique in Australia to quantify basal heat flow showed sensitivities to elevated heat production in Eastern Australia as well as buoyancy from chemically depleted Archean mantle beneath Western Australia (Hasterok & Gard, 2016). This study showed that heat production anomalies approximately 2.5 times the North American reference model could be identified. However, the same methods failed when lithospheric mantle chemical buoyancy was also a significant source of elevation.

OTHERS

The most apparent mass loading process affecting Antarctica is the ice sheets, which are up to 4 kilometres thick in some areas (Fretwell et al., 2013). While data exists for the extant ice sheets, glacial mass-balance (the flux of ice) is something that has been studied by many for a better understanding of climatic processes (Hanna et al., 2013, Rignot et al., 2019, Sasgen et al., 2019). Ice loss occurs over a time scale far smaller than that of isostatic correction, so the ice flux may need to be considered to find an out-of-equilibrium effect.

Flexural contributions to elevation can be on the order of ±1 km (Rubey 2015). Isostatic compensations are calculated as local processes in lithospheric columns (Watts 2011). Strength of the lithosphere prevents local adjustment of these columns to buoyancy, resulting in regional flexure (Watts 2011, Watts 2015) and subsequent isostatic elevation anomalies. The material properties responsible for flexure can be impacted by many variables including composition and thermal state (Wickert 2016, Paxman et al., 2019).

Lastly, mantle convection may cause external forcing on elevation, resulting in a geodynamic contribution to elevation. An ascending convection cell in the aesthenospheric mantle due to thermal perturbation will physically exert an upward force on the overlying lithosphere and raise lithospheric temperature, further contributing to the thermal state. Conversely, a descending convection cell will create subsidence and allow the lithosphere to sink. However, the thermal effect is expressed in thermal isostasy, leaving only the physical pressure effect as an external force in thermal isostatic modelling. Significant heterogeneities in the mantle beneath Western Antarctica have been found via the use of P-wave tomography modelling (Hansen et al., 2014). P-wave velocity perturbations are ± 1% at depths between 150 and 1200 km. Anomalies characterised by slow velocities are interpreted to be significant thermal anomalies, while faster anomalies are present more in East Antarctica and are interpreted as cooler areas.

METHODS

Model Structure

Estimating the thermal contribution to elevation is accomplished in several distinct calculations and making several simplifying assumptions. The broad structure of this model encompasses two lines of computations and is demonstrated in Figure 3. Firstly, a compositional isostatic correction is computed, encompassing ice sheet

mass loading and crustal density. Rearranging Equation (4), assuming flexure and geodynamic effects are negligible in this model (the implications of which are discussed later), thermal elevation can be computed as:

$$\Delta\varepsilon_{thermal} = \varepsilon_{observed} - \Delta\varepsilon_{compositional} - \Delta\varepsilon_{H_2O} \tag{5}$$

where ε denotes elevation. Secondly, thermal conditions of the Antarctic crust are approximated using seismic velocity data and utilising gravity and seismically derived Moho depths and Curie depths to calculate geothermal gradients. These gradients can then be used to calculate thermal elevations as:

$$\varepsilon_{thermal} = \alpha \int_0^{z_{max}} [T(z) - T_{Ref}(z)]dz \tag{6}$$

where ε denotes elevation, α denotes thermal expansivity, z_{max} is the maximum depth of the computed geotherms and *T(z)* are calculated and reference geotherms as labelled. These two thermal elevations are then compared. Pending agreement of the two models via calculation of RMS misfit and comparison of randomly perturbed probability distributions, the geothermal heat flow calculated in the geothermal gradients can then be accepted as a possible geothermal heat flow model. However, in this first pass of the model, probability distributions have not yet been calculated and the baseline model is presented.

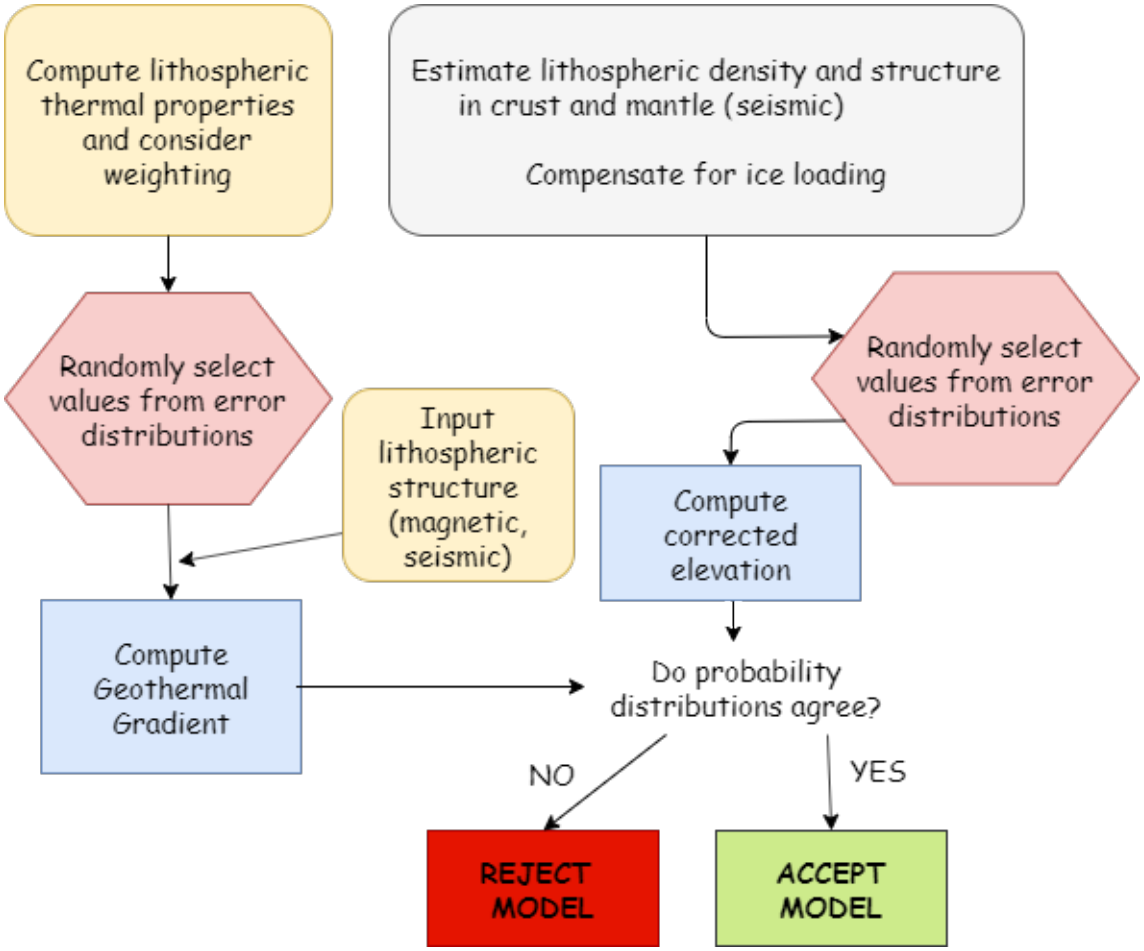

Figure 3: A flow chart illustrating a broad end-goal structure of the model. This flow chart demonstrates the overall structure of the intended model. At this stage, probability distributions from error propagations have not been calculated but are necessary for a more rigorous testing of the model.

Crustal Composition Correction

ICE AND WATER LOADING

Utilising Bedmap2 datasets (Fretwell et al., 2013) for ice thickness and bed rock elevation (Figure 1), an empirical relationship between ice density and depth from data collected by Kuivinen and Koci (1982), coupled with the Mean Value Theorem, is utilised and is given as follows:

$$\rho_{ice} = \frac{1}{h_{ice}} \int_0^{h_{ice}} 3742 + 5624(1 - e^{-0.01525z})dz \tag{7}$$

where ρ is density (kg/m^3) and h is ice thickness. This density combined with the thickness provides corrected elevation (8).

$$\Delta\varepsilon_{ice} = h_{ice}\frac{\rho_{mantle} - \rho_{ice}}{\rho_{mantle}} \tag{8}$$

where $\Delta\varepsilon$ is the difference in elevation defined from the top of the ice sheet to the corrected bedrock surface while density and thickness are labelled as above. Mantle density ρ_{mantle} is assumed to be 3350 kg/m^3, consistent with densities chosen by Haeger et al., (2019). Water loading on the continental shelf is calculated similarly, but with an assumed density of 1030 kg/m^3 for salt water and depth being calculated from the bedrock elevation.

CRUSTAL DENSITY

Shear wave seismic velocity (V_S) data from An et al., (2015) is utilised to approximate the density of the Antarctic crust. Combined with the seismic and gravity derived Moho model from Baranov et al., (2018), this V_S data is utilised to correct compositional variations of density within the crust and compute an isostatic correction as given by:

$$\varepsilon_{crust} = h_{Moho_{average}}(1 - \frac{\rho_{correctedcrust}}{\rho_{mantle}}) - h_{Moho}(1 - \frac{\rho_{crust}}{\rho_{mantle}}) \tag{9}$$

where $\rho_{correctedcrust}$ is arbitrarily set as 2800 kg m^3, similar to Chapman and Hasterok (2011).

V_S vs Density Modelling

Hasterok and Chapman (2007b) utilise a correction for compositional density variations with an empirical pressure wave (V_P) to density relationship. However, limited

shallow V_P data exists for Antarctica, so a relationship between V_S and density has been developed instead.

Behn and Kelemen (2003) utilised thermodynamic modelling to estimate seismic velocities of igneous rocks from geochemical composition data. Hasterok and Webb (2017), and Hasterok et al., (2018) then tested their thermodynamic models with density, producing a relationship between V_P and density. Since both V_P and density produce reliable calibrations to composition, it is reasonable to assume the same can be done for V_S since calculation of both V_S and V_P require the shear modulus and density.

As there are limited data available to calibrate a V_S to density relationship, a similar relationship for V_S is developed utilising the thermodynamically derived estimates for density and V_S from Behn and Kelemen (2003). A relationship utilising a global geochemical database (Gard et al., 2019) to reproduce the same methodology was then produced. The global geochemical database was used to bias the relationship to a more accurate range of rock types to represent the crust than the original data used by Behn and Kelemen (2003). The crust is assumed to be igneous in origin. Models are shown below and the relationship is given in (10).

$$\rho_{crust} = -23424/V_S - 669V_S + 11459 \tag{10}$$

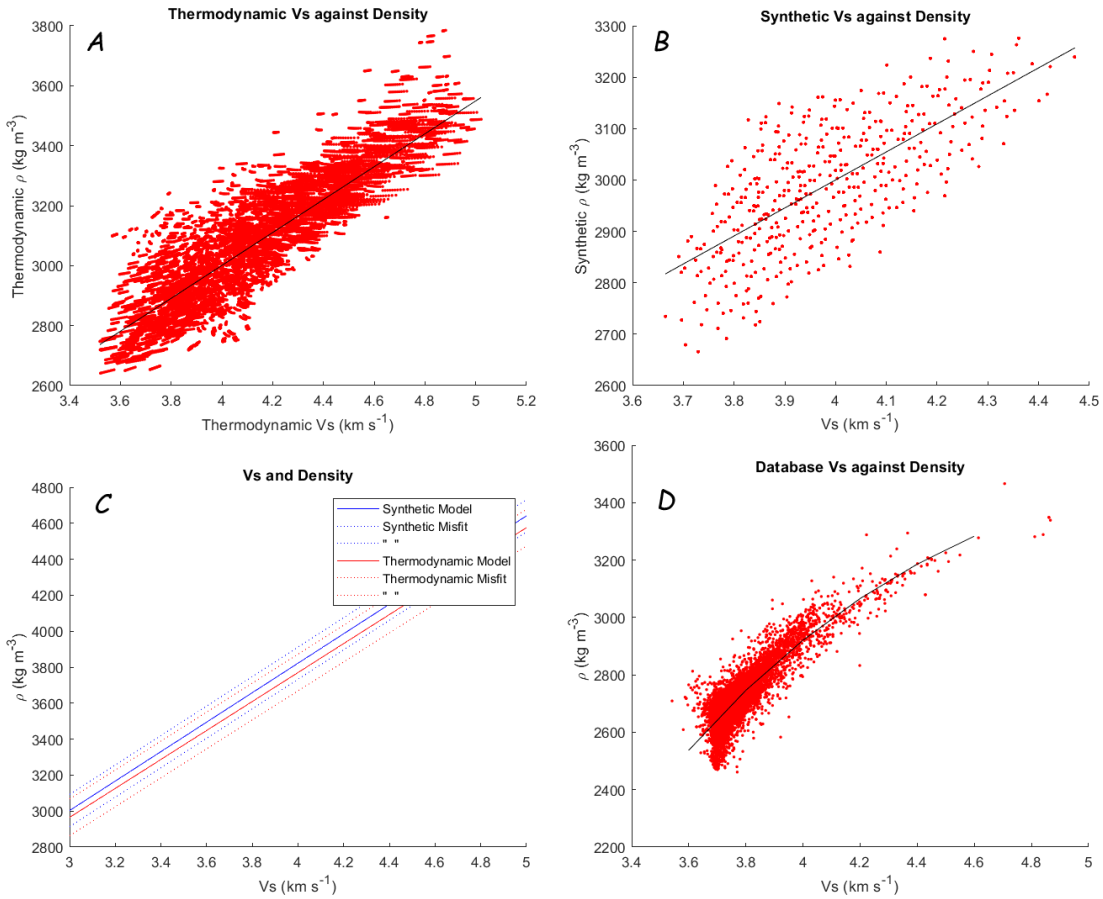

Figure 4: V_S Density modelling. A shows thermodynamic data from Behn and Kelemen (2003), while B is the same sample set but with a synthetic V_S calculated from geochemistry data provided in the same study. C shows the two relationships with RMS misfit, while D is the same synthetic geochemical calculations from the geochemical database. These computations produce (10).

Thermal Modelling

V_S VS HEAT PRODUCTION MODELLING

Seismic velocity can be used to estimate the average heat production in the crust. The global geochemical database is utilised to find an empirical relationship between V_S and heat production (Figure 5). The crust is assumed to be igneous in origin. Modelled geological provinces (Figure 1) of Antarctica are utilised to constrain heat production of different regions. Large natural variability in heat production means that a log-linear relationship was fitted. The computed relationships are listed below in Table 1, with the plot of the regional relationship shown. Where insufficient data

exists to produce an accurate relationship, an Antarctic continent-wide relationship is utilised instead. Provincial relationships with positive slopes were not used as this slope was produced by outliers in data - these provinces instead being reverted to the continental average. It is worth noting that this data is taken from the surface and, as a result, the associated models assume the same seismic velocity to heat production ratio for rocks at depth. This implication is discussed further in the present study.

Figure 5: The log-linear model used for the Antarctic continent-wide V_S Heat Production model. The model (given as the Continental Average in Table 1) is represented by the blue line, with the orange dashed lines being the 95% confidence interval.

Table 1: V_S to Heat Production models. Provinces with positive slopes or insufficient data were not used and instead utilised the continental average. Provinces with insufficient data have their rows populated with '-'. Provinces are also numbered in accordance with Figure 1.

Geological Province	Model Slope	Slope Error	Model Intercept	Intercept Error	Number of Data
Continental Average	-1.6304	0.1404	6.387	0.5493	8883
1. Albany-Fraser-Wilkes Orogen	-	-	-	-	11
2. Rayner Complex	-2.1367	0.2639	0.7544	0.09201	918
3. Fei Craton	1.1591	0.2528	-0.6125	0.1185	546
4. Ross Orogen	-1.0374	0.06229	0.5384	0.02391	3094
5. Antarctandes Forearc	-1.9929	0.5674	0.3499	0.2327	320
6. Amudsen Fold System	-	-	-	-	7
7. Grunehogna	-3.5730	0.4410	1.1960	0.1854	137
8. Napier Complex	-1.3933	0.2704	0.3997	0.1204	481
9. Lambert Rift	-2.1951	0.3045	0.9229	0.1158	467
10. Tanonian Oceanic Arc Terrane	1.0098	0.6823	-0.2783	0.2102	249
11. Mawson Craton	-	-	-	-	67
12. South Polar Basin	-	-	-	-	0
13. West Antarctic Rift	-	-	-	-	23
14. Antarctandes	-1.9111	0.1464	0.7173	0.05153	445
15. Rayner Complex	0.7148	1.5861	0.1843	0.3804	210
16. East African Orogen	-3.3218	0.3704	1.1848	0.1714	642
17. Pinjarra Orogen	-1.5839	0.3498	0.4329	0.1413	459
18. Coats Land	-	-	-	-	44
19. Wilkes Basin	-	-	-	-	5
20. Ruker Craton	-	-	-	-	3
21. West Antarctic Rift	1.0746	1.4712	-0.4669	0.7833	64
22. Erebus Volcanic Province	-2.4619	0.2957	1.1774	0.1224	391
23. Antarctandes	-	-	-	-	23
24. West Antarctic Rift	-	-	-	-	26
25. Ruker Rift	-	-	-	-	0

V_S VS THERMAL CONDUCTIVITY MODELLING

Thermal conductivity can be estimated from seismic velocity. A model based on synthetic V_P estimates from geochemistry has been utilised successfully (Jennings 2017). Similarly, the global geochemical database is also used to compute an empirical relationship between V_S and thermal conductivity. Thermal conductivity is fitted to V_S data with a cubic polynomial for V_S between 3.5 and 5 km/s given as:

$$k_0 = -3.158V_S^3 + 42.339V_S^2 - 187.522V_S + 277.025 \tag{11}$$

where k_0 is thermal conductivity measured at room temperature. This model is shown in Figure 6.

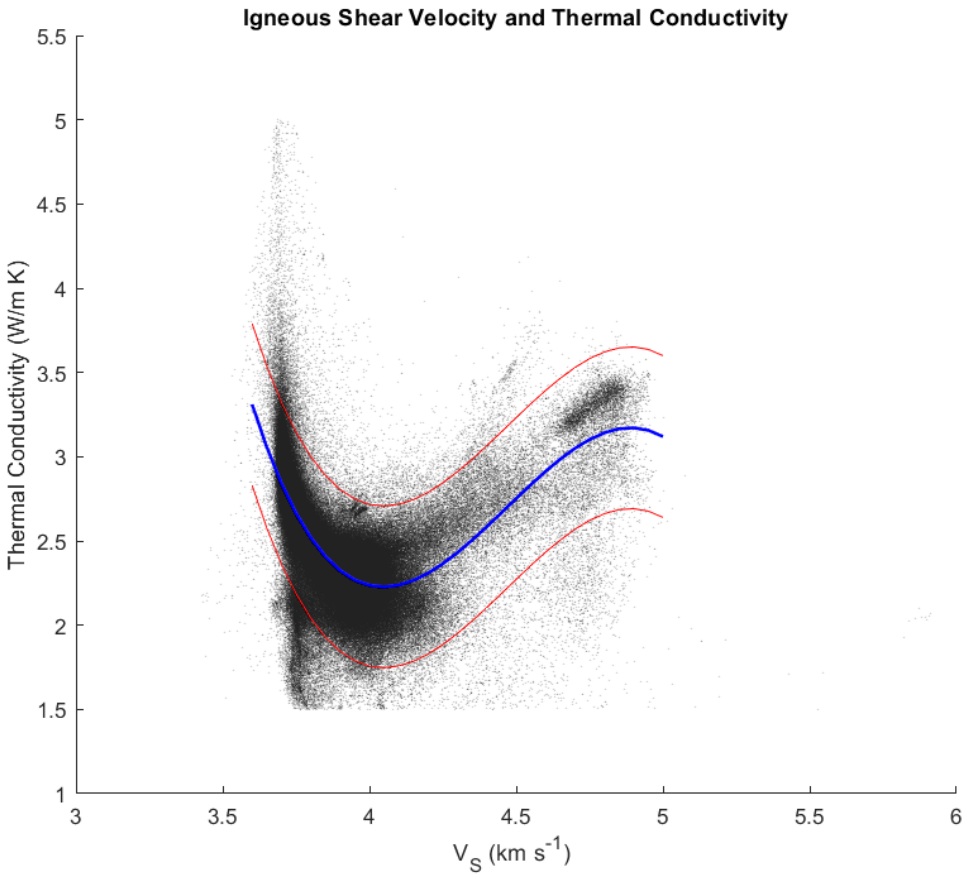

Figure 6: The V_S Thermal Conductivity model. Seismic velocity and thermal conductivity were estimated using the empirical third order polynomial Equation (11). Conductivity estimates below 1.5 W/mK have been excluded because it is rare to find such low values without significant porosity. The centre blue line is the model while the red lines are ± 2 standard deviations.

COMPUTING GEOTHERMS AND THERMAL ELEVATION

Geothermal gradients are modelled using a layered 1-D steady state conductive model. The gradients can be modelled with Equations (2) and (3). Geotherms are calculated to 250 km depth with 1km thick layers.

In all geotherms calculated, mantle heat production is assumed to be 0.02 μWm^{-3}, mantle thermal conductivity is assumed to be 3 Wm^{-1}K^{-1} (consistent with Hasterok and Chapman (2011)), surface temperature is assumed to be 0°C and the mantle adiabat is assumed to occur at 1300°C.

In order to calculate a thermal elevation using Equation (6), a reference geothermal gradient is computed. This reference utilises a mean of the Antarctic Moho depths from Baranov et al., (2018) at 34 km depth. Thermal values assumed for this reference are heat productions of 1 μWm^{-3} for the upper crust (defined as the top 20 km) and 0.2 μWm^{-3} for the lower crust, thermal conductivities of 3.5 Wm^{-1}K^{-1} and 2.5 Wm^{-1}K^{-1} for upper and lower crust respectively and a mantle heat flow of 25 mW/m^2.

With thermal properties estimated with V_S data, preliminary geotherms are calculated. However, as thermal conductivities are measured at room temperatures in the V_S model, the actual thermal conductivity is calculated at the same time as the interface temperature using Newton's Method. These preliminary geotherms are calculated with a mantle heat flow of 20 mW/m^2. A Curie depth model (Martos et al., 2017) is then used to further constrain the geothermal gradients in an iterative process by adjusting the mantle heat flow accordingly, as well as the heat production estimate if geothermal heat flow is above an arbitrarily defined threshold (¿ 90 mW/m^2). This threshold is chosen due to its use as an upper constraint in the model by An et al., (2015). However, as the heat production is constrained by the seismic model, this is adjusted less than the mantle heat flow. The Curie temperature of crustal rock is assumed to be between 550 and 600°C.

RESULTS

Isostatic Corrections

In the V_S density model (Figure 7), some apparent anomalies are present at over 3100 kg/m^3. While higher than expected, these values are not physically unreasonable. Outside of these highs, most values are reasonable with a continental average density of around 2900 kg/m^3.

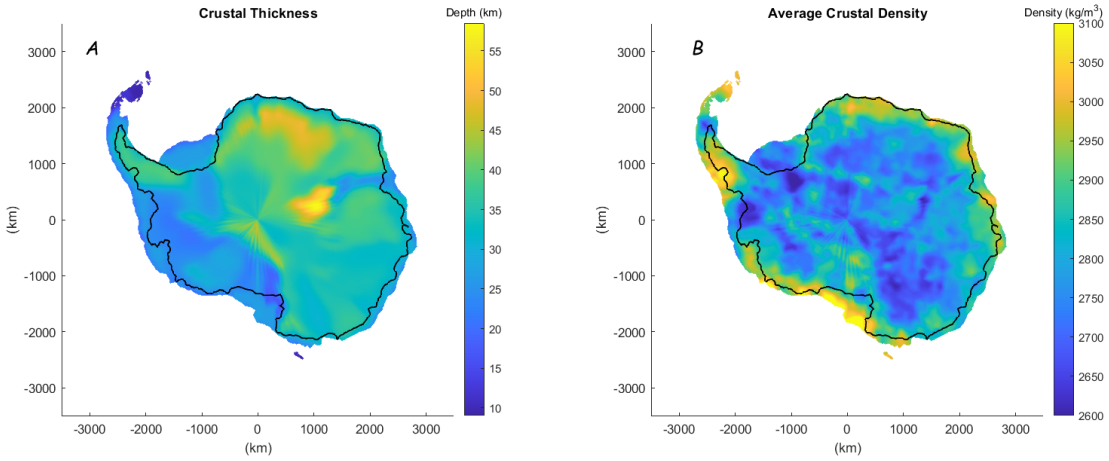

Figure 7: Crustal thickness model on left (Moho depth) and computed average crustal density on right. The Moho depth is modelled by Baranov et al., (2018) while the average crustal density is computed with the relationship given in Equation (10).

As shown in Figure 8, the ice loading correction yields a reasonable magnitude of up to 3 km, while the compositional correction shows anomalously high magnitudes than expected in places, spanning an 8 km difference between its most extreme points. It is noted the density correction shows elevation change in both directions due to both positive and negative density anomalies, while ice loading only removes mass, so the only compensation from ice and water is unidirectional. Additionally, this elevation is defined as the difference between the top of the ice sheet and the resulting surface elevation of corrected bedrock, meaning this correction is applied downward. Positive values in the crustal density isostatic correction indicate low elevation, while negative values indicate high elevation due to the nature of the isostatic calculations.

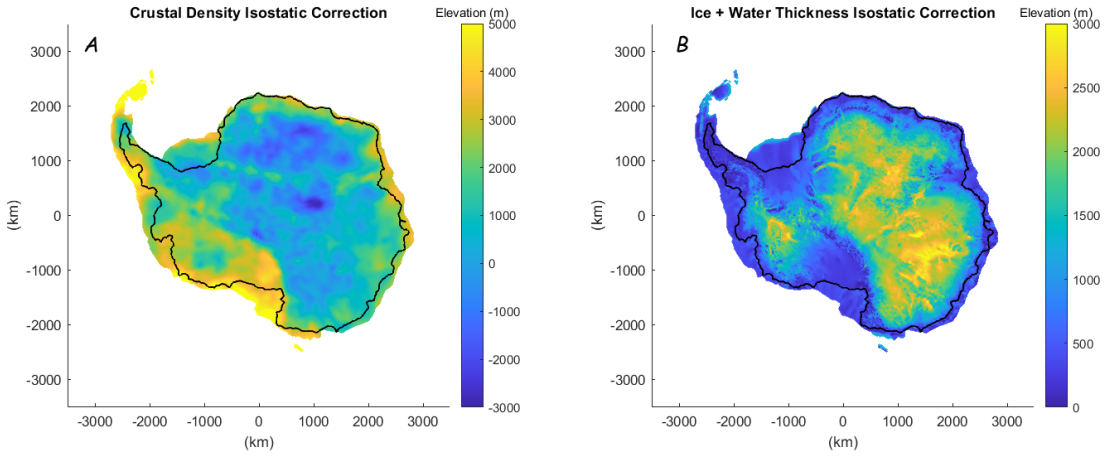

Figure 8: Computed isostatic correction for mass loading of ice sheets and water. Ocean water was considered for continental shelf.

Due to the anomalously high values present in the crustal density isostatic correction, similar high magnitudes are observed in the expected thermal elevation plot. However, regional trends can be observed in Figure 9, with an overall higher elevation noticed in the West and generally lower elevation observed in the East.

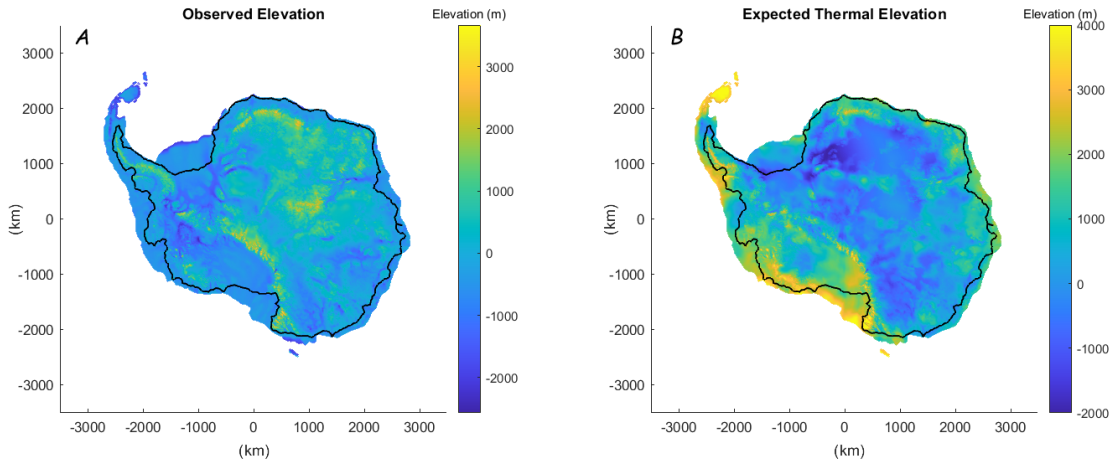

Figure 9: A is the observed bedrock elevation. B is the thermal elevation once correcting for compositional and water effects, as aforementioned in Equation (5). Data for bedrock elevation, ice thickness and water depth was utilised from the Bedmap2 dataset.

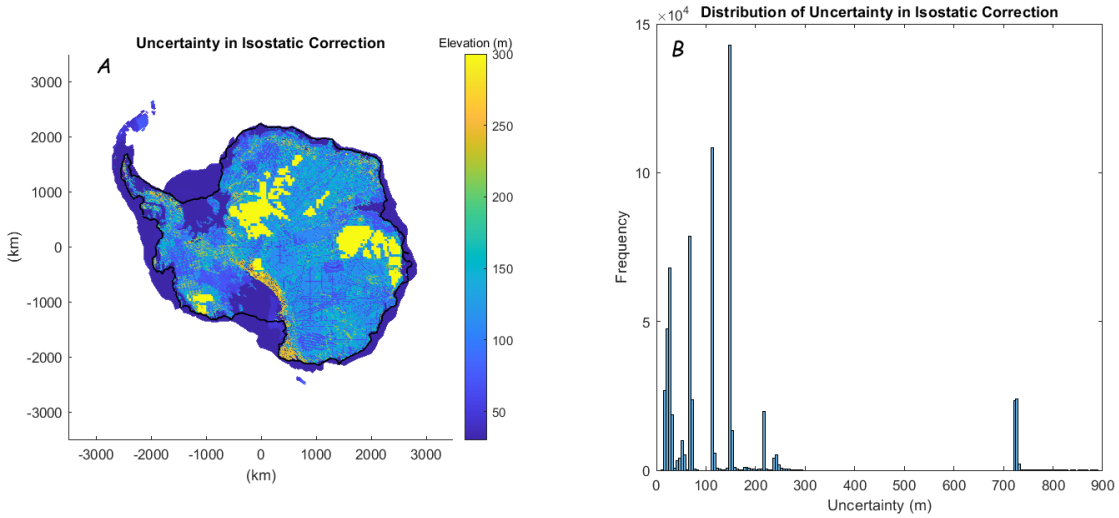

Figure 10: The computed uncertainty in the isostatically derived thermal elevation. A shows the spatial distribution of uncertainty with a compressed colour scale to effectively observe lower uncertainties. B shows the distribution where the true values of the large blocky uncertainties can be seen at over 700m.

The uncertainty present in the isostatic model has large blocky anomalies inherited directly from uncertainties in the Bedmap2 dataset of over 700 m. Outside of these spikes, uncertainty is low at between 30 to 300 m.

Thermal Property Modelling and Geothermal Gradients

Thermal modelling of seismic data produces reasonable results except for a few caveats. The thermal conductivity model in the top 10 km slice shows high thermal conductivities, while provinces 16 and 22 (refer to Table 1) show high heat production values in the top 10 km slice.

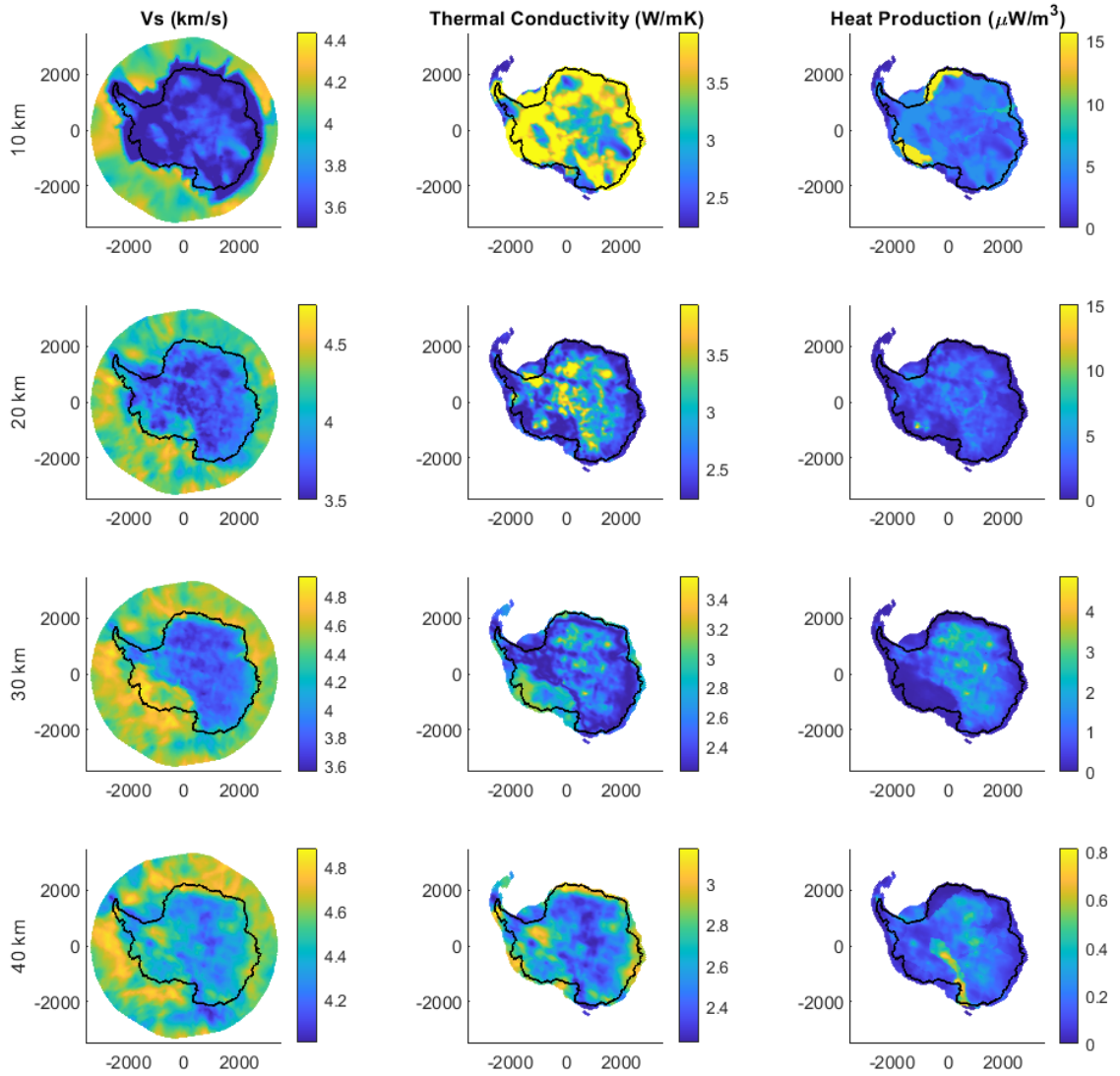

Figure 11: Results from crustal V_S modelling of thermal properties. The input shear velocity data along with thermal conductivity and heat production as described previously. Models are shown for 10 km depth slices.

The preliminary thermal modelling (Figure 12) is notable in its distinct lack of geographical distinctions outside of two particular provinces showing abnormally high heat flow estimates. These anomalies have unrealistic peaks of about 250 mW/m^2. The initial thermal elevation model shows reasonable magnitudes with only negative anomalies on the peninsula and off the coast of the Trans Antarctic Mountains.

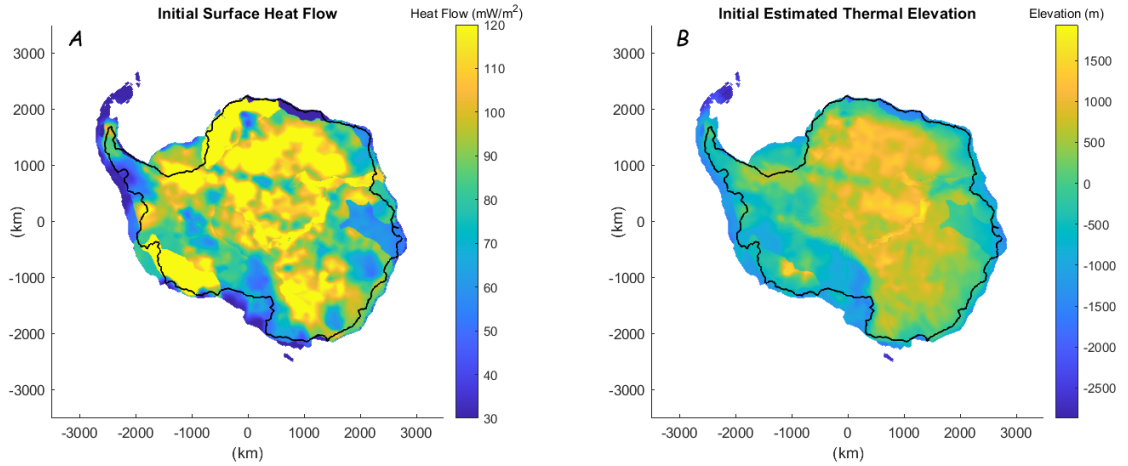

Figure 12: Modelled geothermal heat flow (A) and resulting thermal elevation (B), both before adjusting for Curie depth data. Thermal properties were estimated using models described in Figure 6 and Table 1 before using a steady state geotherm described in Equations (2) and (3) to iteratively produce geotherms. Elevation is then calculated using Equation (6).

After adjusting for Curie depth to produce Figure 13, the average magnitude of the thermal elevation model remains similar. However, the difference between West and East is much more pronounced, with West Antarctica showing more thermal uplift than the East. A direct comparison of the isostatically and thermally modelled elevations is presented in Figure 14.

Figure 14, the thermally calculated elevation model subtracted from the isostatically derived thermal elevation model, shows a Gaussian disstribution with a mean of 196 m and standard deviation of 911 m. The largest positive differences along the Transantarctic Mountains and on the shelf above (in the sense of presented figures) the Antarctic Peninsula, while the largest negative anomaly is present in the West

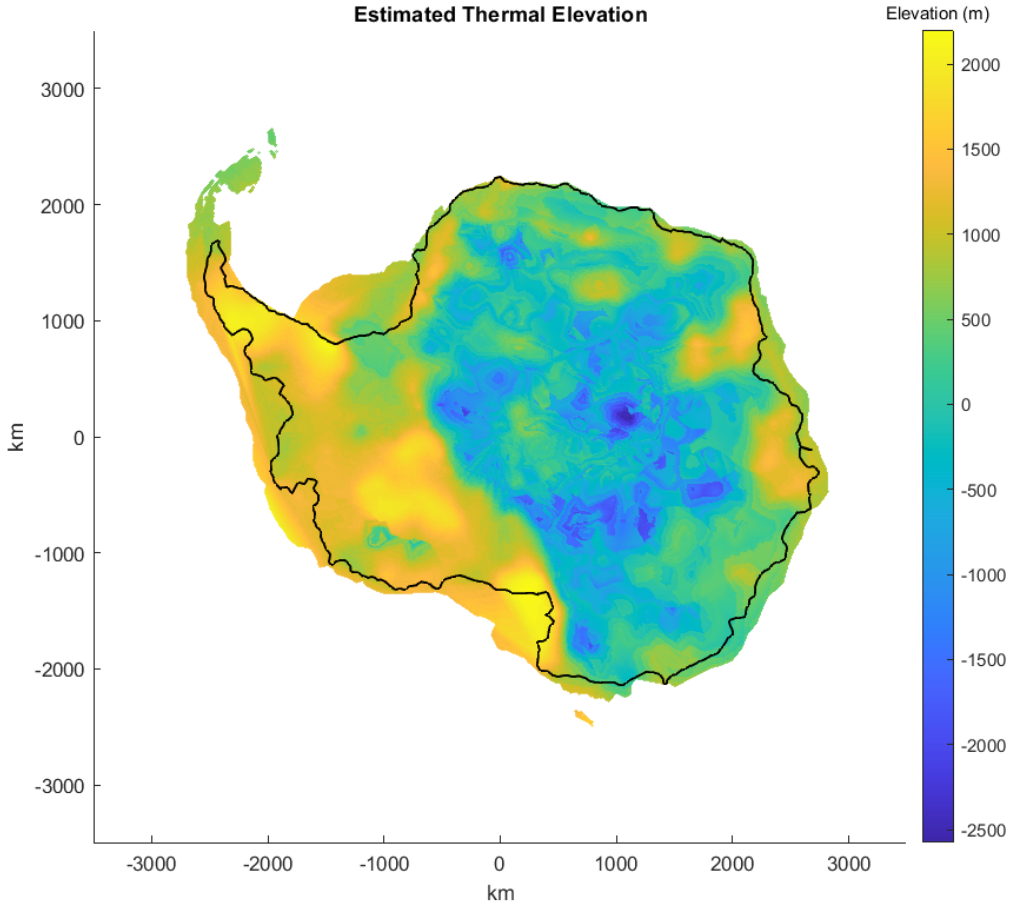

Figure 13: Modelled thermal elevation. This is computed as in Figure 12 B, except with mantle heat flow and heat production constrained by a Curie depth model. Elevation is also computed using Equation (6).

Antarctic Rift adjacent to the Antarctic Peninsula. Aside from these maxima and minima, the differences between the models show no geographical trend.

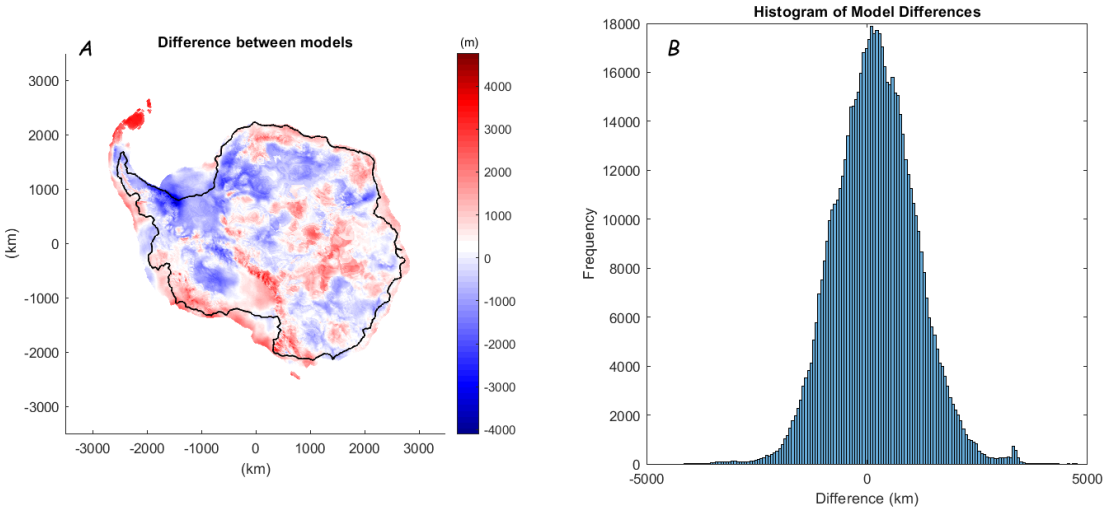

Figure 14: Comparison of the isostatically corrected thermal elevation and the thermally modelled elevation, defined as the difference between the thermal models. A shows the geographical comparison of the two datasets while B shows the distribution of the difference between the datasets. Observe the Gaussian distribution.

After adjusting for Curie depth, the geothermal heat flow model is more reasonable, but still abnormally high. Most of Western Antarctica is above 100 mW/m^2 while East Antarctica averages around 80 mW/m^2. Heat flow sometimes drops as low as 30 mW/m^2 in some areas.

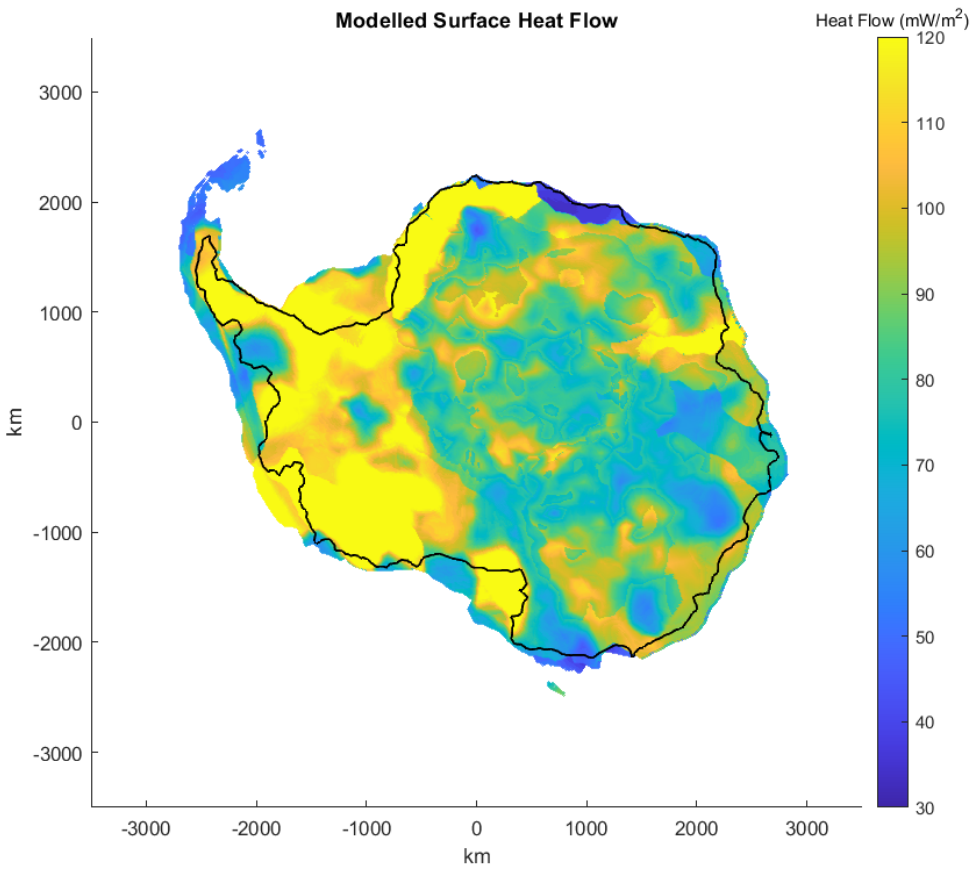

Figure 15: Modelled geothermal heat flow. This is computed as in Figure 12 A, except with mantle heat flow and heat production constrained by a Curie depth model.

DISCUSSION

Model Results

ISOSTATIC MODELLING

While the isostatic correction from ice/water mass loading seems reasonable (Figure 8), the density isostatic correction seems to be unreasonable in places. Investigation of the average density yielded from V_S modelling (Figure 7) shows unnaturally high densities in thin areas of crust - specifically on the Antarctic Peninsula and in the Ross Sea. The Ross Sea, where the West Antarctic Rift system is, may have a higher density due to presence of rift-related basalts (Behrendt et al., 1991). However, due

to the persistence of the anomaly within the starting seismic model, it is unlikely to be caused by rift related basalts. As mentioned, large density anomalies are associated with thinner crust and the top layer of the seismic model. The observed anomaly may be due to the presence of sedimentary/metasedimentary units in the top layer, violating one of the major assumptions of the V_S density model - the assumption of an igneous crust. However, the average density found by the present model used is 2799 kg/m^3 which is a reasonable continental average. Still, this result leaves room for future research in the development of models that incorporate lower velocities for sedimentary units. It is also possible the anomalies are associated with the original V_S model rather than underlying assumptions.

Due to the large magnitudes present in the individual corrections (Figure 8), the resultant isostatically modelled thermal elevation also shows unnaturally large magnitudes that have greater magnitude of thermal elevation difference than previous studies (3 km; Hasterok & Chapman 2007b). While geographical trends seem to be consistent with existent work, some areas in East Antarctica have a lower elevation than expected (up to 1 km) and West Antarctica show magnitudes of up to 5 km (though usually between 3 to 4 km).

The uncertainties in the isostatic model (Figure 10) are too low (maximum 800 m) to explain the difference between the isostatically computed thermal elevation and the thermally computed elevation (Figure 14 - standard deviation of 911 m). While uncertainty on the thermally modelled elevation has not been calculated on this first run, it is essential in making a statistically valid comparison. It is worth noting that, while the uncertainties in the elevation datasets were straightforward, uncertainties present in the V_S density model may have been correlated. As covariance was not taken into account in error propagation, if correlation between coefficients does exist, the overall uncertainty may be underestimated.

THERMAL MODELLING

A clear difference in geothermal heat flow is noticed between East and West, with West Antarctica showing much higher heat flows. The heat flow result consistent with current tectonic knowledge of the area; West Antarctica is known to be much younger with active rifts as opposed to the far older and cratonic East Antarctica. However, the heat flow model produced by this first pass is likely unrealistic. Yielding a continental average geothermal heat flow of 96 mW/m^2 (with the accepted average continental heat flow being 65 mW/m^2; Pollack et al., 1993) indicates thermal properties are likely being drastically overestimated.

Areas of substantially high heat flow include the two geological provinces obersvable in Figures 12 and 15 are the Erebus Volcanic Province and the East African Orogen (Figure 1 and Table 1). Considering the models for geological provincial heat production are based on surface samples and the scarcity of samples across Antarctica, it appears that these provinces are heavily affected by spatial bias of collected geochemical data. This implication is discussed further under the section Sources of Error in Heat Production Modelling.

As shown in Figure 14, the two thermal elevation models are mostly within the range of 2 to 3 km in elevation. While this level of elevation is significant, this deiscrepancy may be accounted for by additional unconsidered elevation sources, discussed further in the section Sources of Error in External Elevation. Overall, this result is not entirely unreasonable and with further work could likely be reduced to a much more reasonable margin of error.

Haeger et al., (2019) utilised seismic models to estimate temperature in the Antarctic lithospheric mantle. These models found temperatures as low as 700°C the East Antarctic lithospheric mantle to depths of 200 km, as shown in Figure 16. While this data has not been used within the model, noting similar geographic trends at

depth supports the differing trends observed between East and West Antarctica in the thermal isostatic model.

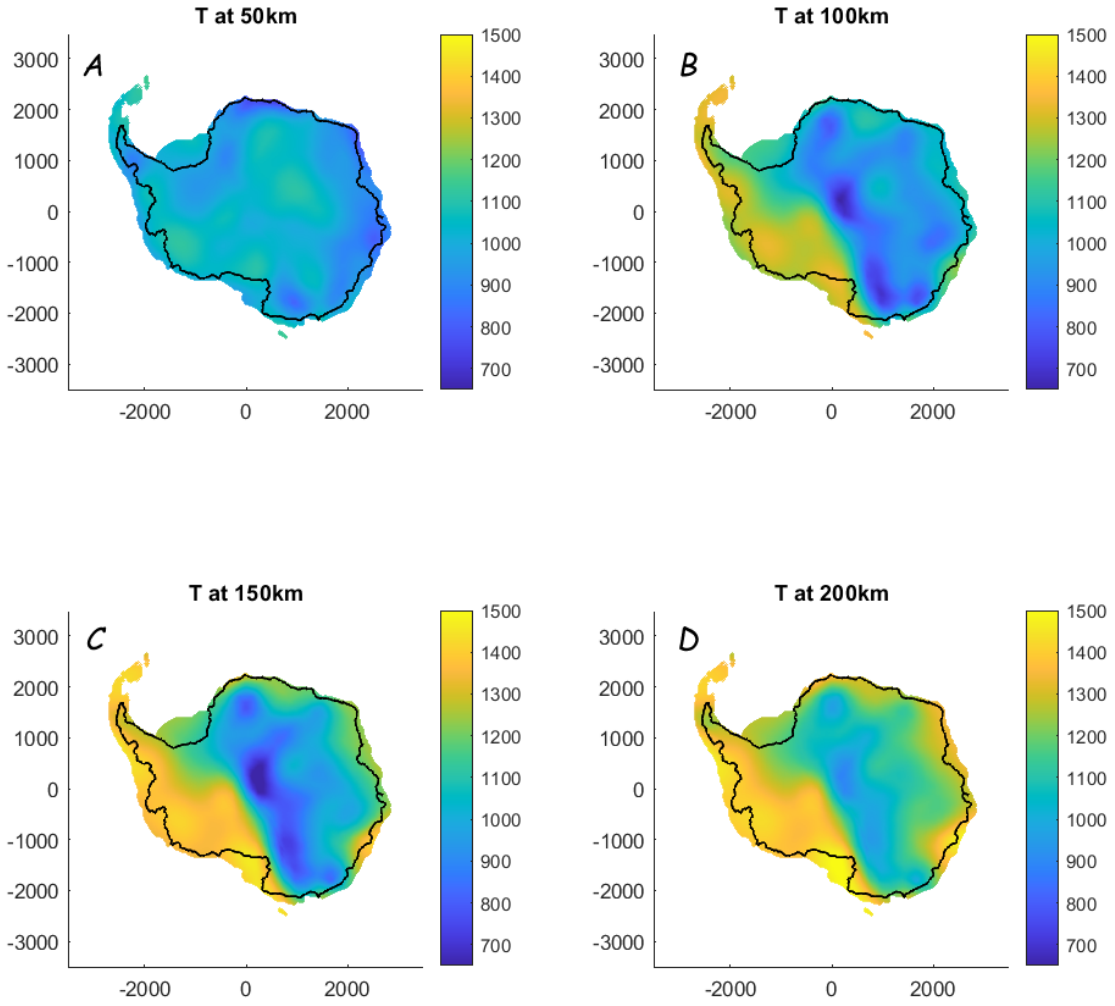

Figure 16: A model for mantle lithosphere temperature at various depths by Haeger et al., (2019). Notice the cold East Antarctic cratonic lithosphere at depth. This may be associated with chemical depletion and thus a negative buoyancy.

Sources of Error

As is typical with most geophysical modelling, certain assumptions have been made for various reasons including availability of data, feasible levels of complexity and to allow for properties to be used as proxies.

EXTERNAL ELEVATION

As previously discussed, flexure and geodynamic mantle processes may account for a significant portion of elevation. Lithospheric mantle variations in density were also not considered and may also account for a significant portion of elevation.

Haeger et al., (2019) utilise seismic models of between 50 and 300 km depth to infer the thermal state of the Antarctic mantle lithosphere. Results show a dense and cold East Antarctic mantle lithosphere, interpreted to be of an Archean age. This interpretation may imply chemical buoyancy in East Antarctic mantle lithosphere is affecting elevation, similar to findings in Western Australia by Hasterok and Gard (2016). Conversely, West Antarctica is shown to have low density and high temperature in its deep lithosphere and is associated with active rifting (Behrendt et al., 1991). The density and temperature data were not considered in the developed model and should be considered in future iterations of this model. The use of this dataset is discussed further below.

Flexure is usually a local feature and is defined as resistance to elevation change due to lateral lithospheric strength (Watts, 2011). Thus, it is likely the total effect may average out over a continental scale. Differences in lithospheric thickness and age, however, will create differences in flexural properties. Flexure can be responsible for elevation differences of ±1 km (Rubey 2015). If flexure is contributing significantly to elevation in Antarctica, one of the fundamental assumptions made in the present model is violated.

Mechanical mantle processes associated with convection and hot spots may cause a similar ±1 km elevation change (Gvirtzman et al., 2016, Goes, 2002). This magnitude, considered with the flexural elevation discussed previously, could well produce the amount of discrepancy in thermal elevation models observed in Figure 14.

P-wave tomography has shown significant anomalies in West Antarctica (Hansen et al., 2014) and are thought to be related to the West Antarctic rift system as

well as hotspot volcanism. While the thermal impact of rifting is accounted for in this model, proposed hotspots and their pressure effects have not been considered. Expansion of the model with mantle models of both V_P and V_S tomography could help reduce this error.

Another observation from the results in Figure 15 is that the geothermal heat flow model is very high on a continental scale yet its associated elevation model generally around 2 km less than that of the isostatically corrected value. This lower elevation strongly suggests external sources of elevation are present in the isostatic thermal model. Further work to constrain the nature of this elevation is necessary.

V_S AND TEMPERATURE

Shear wave velocity is dependent on the shear modulus, which is sensitive to changes in temperature. V_S is often used in tomography to talk about mantle temperature changes (Priestley & McKenzie, 2013). As a result, using V_S to infer properties such as density and heat flow is likely to incorporate thermally induced noise in the data. In future work, seismic inferral of properties would be best done with pressure wave velocities (V_P) as these velocities are less susceptible to thermal effects. As a result, V_P models are likely to produce less thermally biased density estimates. Outside of solely using V_P data, a possible direction could involve a density model that utilises both V_S and V_P in order to simultaneously solve for compositional and thermal properties of the crust. However, as limited shallow V_P data currently exists, incorporation of this data type is likely a long term future direction for this model.

HEAT PRODUCTION MODELLING

Heat production modelling has proven to be challenging in this study. The Erebus Volcanic Province and East African Orogen both drastically overestimate heat flow (Figures 15, 1 and Table 1). As the provincial relationships are based on datapoints from the global geochemical database and Antarctic data is scarce, it appears in

these cases (especially within the Erebus Volcanic Province) the data points within these provinces suffer from spatial bias of a singular geological feature. Expansion of geochemical data from these provinces would be the ideal solution, but may not be feasible. Future models may incorporate these data weighted against the continental average in an attempt to remove the bias from the sampled feature.

Another assumption present in the methodology of this study is the depth of heat production from the V_S to heat production model. Samples in the geochemical database are collected from the surface. Brady et al., (2006) utilise geochemical and geobarometric analyses to produce a relationship between heat production and depth for the Sierra Nevada Batholith and find, despite a lower surface heat production due to a volcanic pile, the upper crust beneath the volcanics has the highest heat production of around 3.5 μW/m^3, dropping drastically to around 1 μW/m^3 at around 15 km depth. Thus, it is likely the seismic model of heat production given in Figure 5 may overestimate heat production at the depths of mid to lower crust.

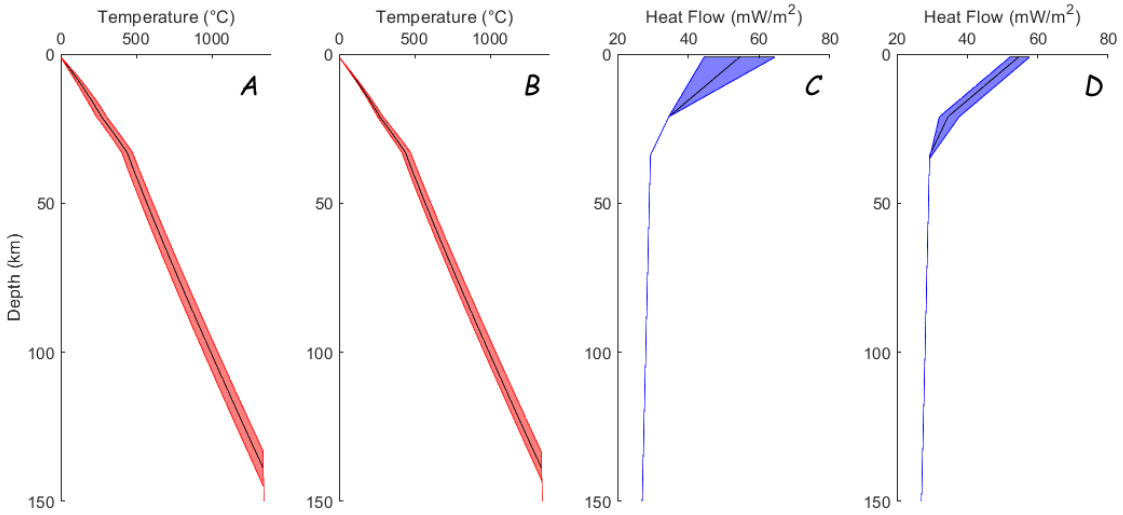

Figure 17: Plots demonstrating the reference geothermal gradient and heat flow with depth and their sensitivities to change in heat production. A shows the perturbed geotherm to ± 50% upper crustal heat production, while B demonstrates the perturbed geotherm to ± 50% lower crustal heat production. Figures C and D demonstrate the same perturbations respectively, but demonstrate the impact on heat flow.

However, in the estimation of geothermal heat flow from geothermal gradients, it is important to consider the sensitivities of geotherms and geothermal heat flux to change in heat production at depth. The reference geotherm utilised in producing the thermal elevation in Figure 13 has been taken and had heat productions in the upper and lower crust perturbed to demonstrate the impact (Figure 17) While the lower crustal heat production still impacts heat flow, the greater effect comes from shallow crustal values.

IGNEOUS MODELLING

Igneous and metaigneous rocks make up a majority of continental crust by volume - up to 95% by some estimates, so models are based on the assumption of an igneous crust. However, not all crustal rocks are igneous. Investigation in the geochemical database indicated metaigneous rocks tend to behave similarly to igneous rocks with regards to physical properties such as density, seismic velocities and thermal properties, but sedimentary and metasedimentary rocks do not. This discrepancy is especially true with thermal properties such as heat production and thermal conductivity. Thus, provinces with a significant fraction of sedimentary-derived material may result in significant errors in isostatic calculations resulting from V_S to property conversions.

Baranov et al., (2018) present a seismic model of sediment thickness across Antarctica, utilising data from multiple previous local scale studies. This model shows a major basin associated with the West Antarctic Rift underneath the Filchner-Ronne Ice Shelf of up to 14 km depth. This basin is consistent with an anomaly characterised by a slow velocity in the 10 km slice of the dataset (Figure 11), implying a violation of the igneous composition assumption present in this modelling. Sedimentary basins of up to 6 km depth are present throughout the rest of the West Antarctic Rift system (Baranov et al., 2018) but do not appear to correlate with other anomalies in the present model.

GEOTHERMAL GRADIENT CONSTRAINTS

Geothermal gradients may be restrained at depth with the use of geophysical proxies (Figure 18). These restraints include Curie depth modelling from magnetic data, electrical conductivity, seismic tomography and sub-Moho normalised V_P (V_{Pn}) (Hasterok et al., 2019). Non geophysical methods to constrain geotherms include measurement of surface heat flow and heat production (not viable in this model as discussed previously) and thermobarometric analysis of xenoliths (Hasterok and Chapman 2011, Hasterok et al., 2019).

Mantle tomography has been the subject of extensive research in the Antarctic context but still suffers from uncertainties due to compositional variations. Hansen et al., (2014) utilise V_P tomography to identify fast anomalies in East Antarctica and slow anomalies in West Antarctica. Depths determined depend heavily on the modelling method but are at least as deep as 300 km and up to 800 km. These anomalies could be utilised in future research to further constrain geotherms at depth. Though xenolith thermobarometry has been utilised successfully in modelling geothermal gradients (Hasterok and Chapman, 2011), it requires physical access to said xenoliths, limiting its use in Antarctica. However, xenolith thermobarometry may indicate palaeo-geotherms that are not representative of current day ones. Electrical conductivity data is rare in Antarctica (Hasterok et al., 2019). Aside from its rarity, it also has difficulty in distinguishing temperature effects from hydration and melt effects.

The shallowest subsurface thermal feature is the Curie depth, which often comes with high uncertainties. The Curie depth model utilised for this study (Martos et al., 2017) has a maximum uncertainty of 8.9 km with a mean of approximately 3 km. The importance of the Curie depth in this model's estimation of surface heat flow is demonstrated directly by Figures 12, 13 & 15.

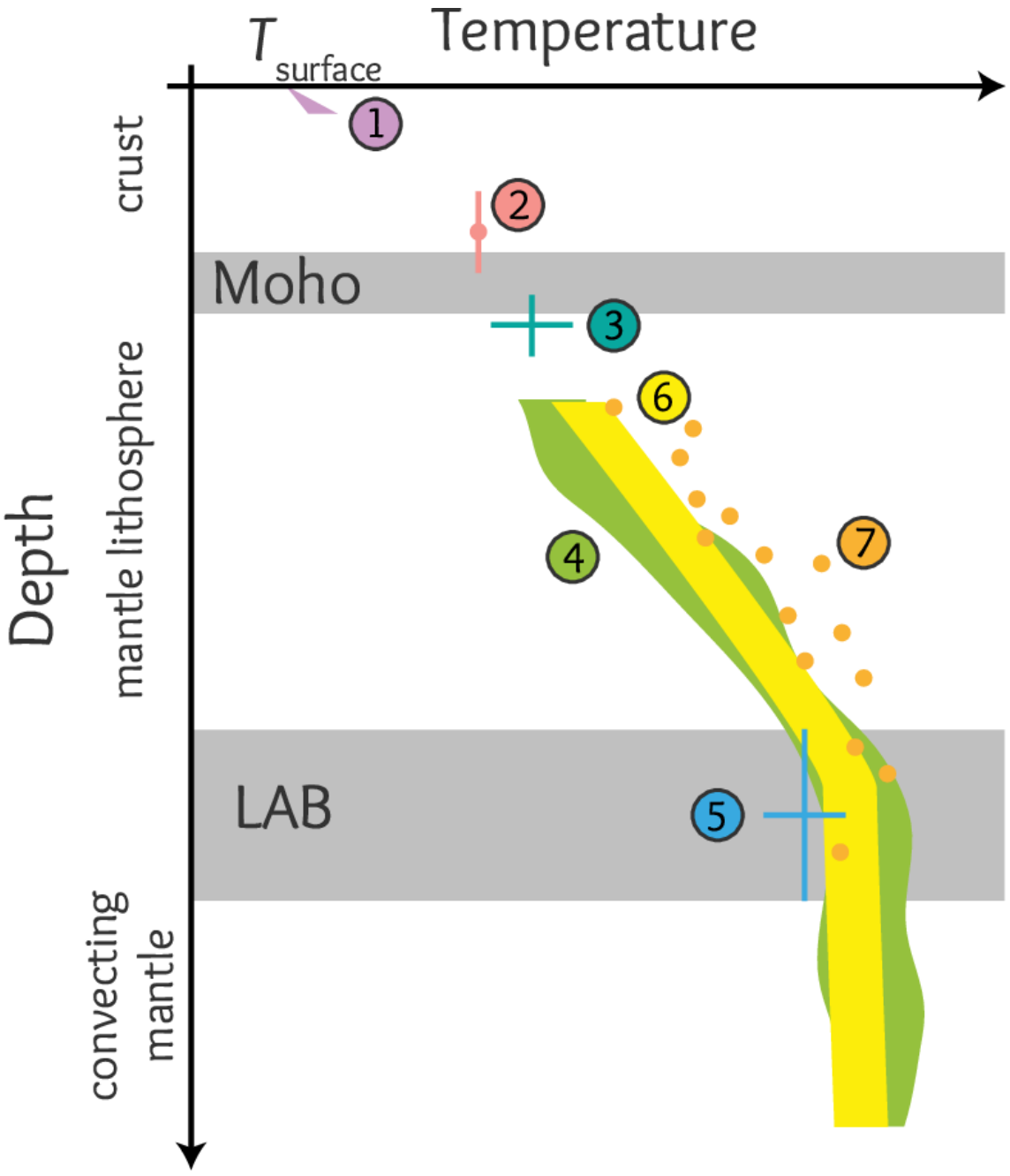

Figure 18: A plot showing geophysical proxies for various depths in constraining geothermal gradients. Proxies are labelled numerically — 1. geothermal heat flux, 2. magnetics (Curie Depth), 3. Sub-Moho P_n velocity, 4. Seismic tomography, 5. Receiver functions (seismic lithosphere - aesthenosphere boundary), 6. Electrical conductivity and 7. Xenolith thermobarometry.

Future Directions

Future directions for this model can be divided into (a) short term improvements with existent datasets and (b) long term improvements pending collection of new data. One of the proposed advantages of utilising thermal isostasy to model surface heat flow is the variety of data types that can be utilised to constrain thermal properties of the lithosphere, so as more data becomes available, thermal isostatic modelling will improve.

Existing geophysical data not directly utilised in this model include mantle tomography (V_S and V_P; Hansen et al., 2014; An et al., 2015; Haeger et al., 2019) and gravity surveys (Pappa et al., 2019; Scheinert et al., 2016; Haeger et al., 2019). Utilising mantle tomography to correct for thermal and compositional variations would allow for further constraining of the crustal thermal elevation, permitting further improvement of the isostatic model and thus the surface heat flow model. Gravity surveys may also prove useful in conjunction with seismic velocity to density conversions to create a more robust density model that is less susceptible to errors associated with either method (thermal perturbations for seismic velocities, while the seismic to density conversion may help with inverse modelling of gravity data).

Haeger et al., (2019) in particular present in depth study of the Antarctic lithosphere at depth, including models of compositional variations and temperature derived from gravity data and seismic models. Integration of Haeger et al., (2019) data into this model is one of the short term future directions of the present model, as the only current constraint on the geothermal gradient after modelling thermal features is the Curie depth model. This mantle temperature model will also help account for mantle features currently not accounted for in the current geothermal model.

V_S models utilised in this study were based on igneous rocks with velocities rarely dropping below 3.6 km/s. However, shear velocities in the utilised seismic model often drop below 3.6 km/s, especially closer to the surface. Another short term di-

rection in this model involves developing sedimentary based models for low velocities and shallow depths, incorporating porosity and depth estimates. These parameters would likely offset anomalies noticed in the shallow components of V_S models used in this study (Figure 11). Incorporating the seismic model of sediment thickness from Baranov et al., (2018) would aid this process greatly.

Additionally, as more Antarctic geophysical surveys are undertaken and more data becomes available, more data can be integrated to create a diversely restrained geothermal gradient to help improve the surface heat flow model, including data shown in Figure 18.

CONCLUSION

Thermal isostasy is used to produce a surface heat flow model for Antarctica. A series of isostatic corrections utilising geophysical proxies are used to isolate the thermal component of elevation which is then used to verify a thermal model formed from remote geophysical data.

Isostatic corrections for ice sheets performed well due to the inherent simplicity of the system. Ice sheets and seawater were found to be responsible for up to 3 km of elevation difference. The crustal density isostatic correction performed relatively well with a few issues - likely due to non-igneous rocks in the top layer of the crust, anomalies within the starting velocity model or both. This correction calculated an average crustal density of 2799 kg/m^3, very close to the continental average, and was responsible for ± 4 kilometres of isostatic compensation. The magnitude of this correction is much larger than most seen in previous work, which is indicates that refinement is needed.

The V_S to thermal conductivity conversion model developed performed well when combined with iterative methods to calculate thermal conductivity at depth, only showing issues with surface V_S values. With the exception of insufficient data in

areas and some provinces producing anomalously high heat production values, the V_S to heat production also performed reasonably, though it is suspected this model overestimates heat production. The geothermal heat flow model produced suggests this overestimation, with a regional average of 92 mW/m^2. This result is far higher than the accepted continental average (around 65 mW/m^2). However, even with elevated heat flow estimates, the thermal elevation estimate from this method seems reasonable with a magnitude of $\pm$2 km excluding some extreme anomalies. With further work to restrain the geothermal gradients and isostatic corrections further, this method will produce far more reasonable results.

ACKNOWLEDGEMENTS

My deepest gratitude goes out to my supervisor Derrick Hasterok for his unending patience and support throughout the course of this project. I would also like to thank Simon Wilcocks and Samuel Jennings whose work and support greatly improved many aspects of this study. A majority of this project would not have been possible without the global geochemical database supported by the ARC Discovery Scheme, grant number DP180104074. My thanks also go out to Martin Hand whose geological advice was indispensable. Lastly, to Celina Sanso, Romana Dew, George Symonds and Teagan Romyn, whose invaluable suggestions improved the quality of this paper, thank you.

REFERENCES

The people you are quoting! If you can find a better way of doing the references (i.e. linking Endnote with this), then please change this! I first put in all my references into word, then changed the author names to ALL CAPS, then copied and pasted into here.

An, M., WIENS, D. A., ZHAO, Y., FENG, M., NYBLADE, A., KANAO, M., Lévêque, J. J. (2015a). Temperature, lithosphere-asthenosphere boundary, and heat flux beneath the Antarctic Plate inferred from seismic velocities. Journal of Geophysical Research: Solid Earth, 120(12), 8720-8742. doi:10.1002/2015JB011917

AN, M., WIENS, D. A., ZHAO, Y., FENG, M., NYBLADE, A. A., KANAO, M., LEVEQUE, J. J. (2015b). S-velocity model and inferred Moho topography beneath the Antarctic Plate from Rayleigh waves. Journal of Geophysical Research: Solid Earth, 120(1), 359-383. doi:10.1002/2014JB011332

BARANOV, A., & MORELLI, A. (2013). The Moho depth map of the Antarctica region. Tectonophysics, 609, 299-313. doi:10.1016/j.tecto.2012.12.023

BARANOV, A., TENZER, R., BAGHERBANDI, M. (2018). Combined Gravimetric–Seismic Crustal Model for Antarctica. Surveys in Geophysics, 39(1), 23-56. doi:10.1007/s10712-017-9423-5

BEHN, M. D., KELEMEN, P. B. (2003). Relationship between seismic P-wave velocity and the composition of anhydrous igneous and meta-igneous rocks. 4(5). doi:10.1029/2002gc000393

BEHRENDT, J. C., LEMAUSRIER, W. E., COOPER, A. K., TESSENSOHN, F., TREHU, A., DAMASKE, D. (1991). Geophysical studies of the West Antarctic Rift System. 10(6), 1257-1273. doi:10.1029/91tc00868

BLACKMAN, D. K., VON HERZEN, R. P., LAWVER, L. A. (1987). Heat flow and tectonics in the western Ross Sea, Antarctica. The Antarctic Continental Margin: Geology and Geophysics of the Western Ross Sea, 5 B, 179-189.

BLOCK, A. E., BELL, R. E., STUDINGER, M. (2009). Antarctic crustal thickness from satellite gravity: Implications for the Transantarctic and Gamburtsev Subglacial Mountains. Earth and Planetary Science Letters, 288(1-2), 194-203. doi:10.1016/j.epsl.2009.09.022

BRADY, R., DUCEA, M., KIDDER, S., SALEEBY, J. (2006). The distribution of radiogenic heat production as a function of depth in the Sierra Nevada Batholith, California. LITHOS, 86, 229-244. doi:10.1016/j.lithos.2005.06.003

Bücker, C. J., Jarrard, R. D., Wonik, T. (2001). Downhole temperature, radiogenic heat production, and heat flow from the CRP-3 drillhole, Victoria Land Basin, Antarctica. Terra Antarctica, 8(3), 151-159.

BÜCKER, C. J., WONIK, T., JARRARD, R. (2000). The temperture and salinity profile in CRP-2/2A, Victoria Land Basin, Antarctica. Terra Antarctica, 7(3), 255-259.

CHAPMAN, D. S., HASTEROK, D. (2011) Isostasy, Thermal. In: Vol. Part 5. Encyclopedia of Earth Sciences Series (pp. 662-668): Springer Netherlands.

Dziadek, R., Gohl, K., Kaul, N., Science Team of Expedition, P. S. (2019). Elevated Geothermal Surface Heat Flow in the Amundsen Sea Embayment, West Antarctica. Earth and Planetary Science Letters, 506, 530-539. doi:10.1016/j.epsl.2018.11.003

ELBARBARY, S., ABDEL ZAHER, M., MESBAH, H., EL-SHAHAT, A., EMBABY, A. (2018). Curie point depth, heat flow and geothermal gradient maps of Egypt deduced from aeromagnetic data. Renewable and Sustainable Energy Reviews, 91, 620-629. doi:10.1016/j.rser.2018.04.071

FRETWELL, P., PRITCHARD, H. D., VAUGHAN, D. G., BAMBER, J. L., BARRAND, N. E., BELL, R., . . . ZIRIZOTTI, A. (2013). Bedmap2: Improved ice bed, surface and thickness datasets for Antarctica. Cryosphere, 7(1), 375-393. doi:10.5194/tc-7-375-2013

GARD, M., HASTEROK, D., HALPIN, J. A. (2019). Global whole-rock geochemical database compilation. Earth System Science Data, 11(4), 1553-1566. doi:10.5194/essd-11-1553-2019

GOES, S. (2002). Thermal structure of the North American uppermost mantle inferred from seismic tomography. Journal of Geophysical Research, 107(B3). doi:10.1029/2000jb000049

GVIRTZMA, Z., FACCENNA, C., BECKER, T. W. (2016). Isostasy, flexure, and dynamic topography. Tectonophysics, 683, 255-271. doi:10.1016/j.tecto.2016.05.041

HAEGER, C., KABAN, M. K., TESAURO, M., PETRUNIN, A. G., MOONEY, W. D. (2019). 3-D Density, Thermal, and Compositional Model of the Antarctic Lithosphere and Implications for Its Evolution. Geochemistry, Geophysics, Geosystems, 20(2), 688-707. doi:10.1029/2018gc008033

HANSEN, S. E., GRAW, J. H., KEYNON, L. M., NYBLADE, A. A., WIENS, D. A., ASTER, R. C., . . . WILSON, T. (2014). Imaging the Antarctic mantle using adaptively parameterized P-wave tomography: Evidence for heterogeneous structure beneath West Antarctica. Earth and Planetary Science Letters, 408, 66-78. doi:10.1016/j.epsl.2014.09.043

HASTEROK, D., CHAPMAN, D. S. (2007a). Continental Thermal Isostasy: 1. Methods and Sensitivity. Journal of Geophysical Research: Solid Earth, 112(6). doi:10.1029/2006JB004663 10.1029/2006JB004664;

HASTEROK, D., CHAPMAN, D. S. (2007b). Continental Thermal Isostasy: 2. Application to North America. Journal of Geophysical Research: Solid Earth, 112(6). doi:10.1029/2006JB004664 10.1029/2006JB004663;

HASTEROK, D., CHAPMAN, D. S. (2011). Heat Production and Geotherms for the Continental Lithosphere. Earth and Planetary Science Letters, 307(1-2), 59-70. doi:10.1016/j.epsl.2011.04.034

HASTEROK, D., GARD, M. (2016). Utilizing Thermal Isostasy to Estimate Sub-Lithospheric Heat Flow and Anomalous Crustal Radioactivity. Earth and Planetary Science Letters, 450, 197-207. doi:10.1016/j.epsl.2016.06.037

HASTEROK, D., GARD, M., HAND, M., HALPIN, J. A., POLLETT, A., MCLAREN S., . . . LINKE, M. (2019). Constraining geothermal heat flux beneath ice sheets using thermal isostasy. Poster presented at the AGU, San Francisco, CA.

JORDAN, T. A., MARTIN, C., FERRACIOLI, F., Matsuoka, K., Corr, H., FORSBERG, R., . . . SIEGETR, M. (2018). Anomalously high geothermal flux near the South Pole. Scientific Reports, 8(1), 16785. doi:10.1038/s41598-018-35182-0

KUIVINEN, K. C., KOCI, B. R. (1982). South Pole ice core drilling, 1981 - 1982. Antarctic Journal of the United States, 17(5), 89-91.

MARTOS, Y. M., CATALAN, M., JORDAN, T. A., GOLYNSKY, D., EAGLES, G., VAUGHAN, D. G. (2017). Heat Flux Distribution of Antarctica Unveiled. Geophysical Research Letters, 44(22), 11,417-411,426. doi:10.1002/2017gl075609

MAULE, C. F., PURUCKER, M. E., OLSEN, N., MOSEGAARD, K. (2005). Geophysics: Heat flux anomalies in Antarctica revealed by satellite magnetic data. Science, 309(5733), 464-467. doi:10.1126/science.1106888

O'DONELL, J. P., STUART, G. W., BRISBOURNE, A. M., SELWAY, K., YANG, Y., NIELD, G. A., WINBERRY, J. P. (2019). The Uppermost Mantle Seismic Velocity Structure of West Antarctica from Rayleigh Wave Tomography: Insights into Tectonic Structure and Geothermal Heat Flow. Earth and Planetary Science Letters, 522, 219-233. doi:10.1016/j.epsl.2019.06.024

PAPPA, F., EBBING, J., FERRACIOLI, F. (2019). Moho Depths of Antarctica: Comparison of Seismic, Gravity, and Isostatic Results. Geochemistry, Geophysics, Geosystems, 20(3), 1629-1645. doi:10.1029/2018gc008111

PAXMAN, G. J. G., JAMIESON, S. S. R., FERRACIOLI, F., BENTLEY, M. J., ROSS, N., WATTS, A. B., YOUNG, D. A. (2019). The Role of Lithospheric Flexure in the Landscape Evolution of the Wilkes Subglacial Basin and Transantarctic Mountains, East Antarctica. Journal of Geophysical Research: Earth Surface, 124(3), 812-829. doi:10.1029/2018JF004705

POLLACK, H., HURTER, S., JOHNSON, J. (1993). Heat Flow from the Earth's Interior: Analysis of the Global Data Set. Reviews of Geophysics, 31, 267-280. doi:10.1029/93RG01249

POLLETT, A., HASTEROK, D., Raimondo, T., HALPIN, J. A., HAND, M., Bendall, B., McLaren, S. (2019). Heat Flow in Southern Australia and Connections with East Antarctica. Geochemistry, Geophysics, Geosystems.

PRIESTLEY, K., MCKENZIE, D. (2013). The relationship between shear wave velocity, temperature, attenuation and viscosity in the shallow part of the mantle. Earth and Planetary Science Letters, 381, 78-91. doi:https://doi.org/10.1016/j.epsl.2013.08.022

QUINTERO, W., CAMPOS-EENRIQUEZ, O., HERNANDEZ, O. (2019). Curie point depth, thermal gradient, and heat flow in the Colombian Caribbean (northwestern South America). Geothermal Energy, 7(1). doi:10.1186/s40517-019-0132-9

RIGNOT, E., MOUGINOT, J., SCHEUCHL, B., VAN DEN BOREKE, M., VAN WESSEM, M. J., MORLIGHEM, M. (2019). Four Decades of Antarctic Ice Sheet Mass Balance from 1979-2017. Proc Natl Acad Sci U S A, 116(4), 1095-1103. doi:10.1073/pnas.1812883116

RUBEY, M. (2015). Earth's dynamic topography evolution during the last 200 Myr: Insights from mantle convection models with imposed plate motions. (PhD Doctorate), University of Sydney.

SASGEN, I., KONRAD, H., HELM, V., GROSFELD, K. (2019). High-Resolution Mass Trends of the Antarctic Ice Sheet Through a Spectral Combination of Satellite Gravimetry and Radar Altimetry Observations. Remote Sensing, 11(2). doi:10.3390/rs11020144

SCHEINERT, M., FERRCAIOLI, F., SCHWABE, J., BELL, R., STUDINGER, M., DAMASKE, D., RICHTER, T. D. (2016). New Antarctic Gravity Anomaly Grid for Enhanced Geodetic and Geophysical Studies in Antarctica. Geophys Res Lett, 43(2), 600-610. doi:10.1002/2015GL067439

SHAPIRO, N. M., RITZWOLLER, M. H. (2004). Inferring surface heat flux distributions guided by a global seismic model: Particular application to Antarctica. Earth and Planetary Science Letters, 223(1-2), 213-224. doi:10.1016/j.epsl.2004.04.011

SHEPERD, A., IVINS, E. R., GERUO, A., BARLETTA, V. R., BENTLEY, M. J., BETTADPUR, S., . . . ZWALLY, H. J. (2012). A Reconciled Estimate of Ice-Sheet Mass Balance. Science, 338(6111), 1183-1189. doi:10.1126/science.1228102

WATTS, A. B. (2011) Isostasy. In: Vol. Part 5. Encyclopedia of Earth Sciences Series (pp. 647-662): Springer Netherlands.

WICKERT, A. D. (2016). Open-source modular solutions for flexural isostasy: GFlex v1.0. Geoscientific Model Development, 9(3), 997-1017. doi:10.5194/gmd-9-997-2016